Mountain-Top-to-Mountain-Top Optical Link Demonstration: Part I

A. Biswas[1] and M. W. Wright[1]

A mountain-top-to-mountain-top optical link was demonstrated between JPL's Table Mountain Facility (TMF), Wrightwood, California, and Strawberry Peak (SP), Lake Arrowhead, California, during the months of June, August, and September of 2000. The bidirectional laser link was nearly horizontal at an altitude of 2 km and spanned a range of 46.8 km. The 780-nm beacon laser transmitted from TMF comprised eight co-propagating mutually incoherent laser beams. The normalized variance or scintillation index (SI) of the individual beacon lasers measured by recording the signal received through 8.50-cm-diameter spotting telescopes on three different nights (June 28–30, 2000) was 1.05 ± 0.2, 1.76 ± 0.6, *and* 0.96 ± 0.24, *respectively. These measurements agreed with values predicted by a heuristic model. The SI of the signal received at SP was found to decrease progressively with an increasing number of beams, and a factor of 3 to 3.5 reduction was achieved for all eight beams. The beam divergence determined by mapping out the point spread function of a few of the individual laser footprints received at SP was 85 to 150* μ*rad, compared to a design goal of 120* μ*rad. The 852-nm communications laser beam received at TMF through a 60-cm-diameter telescope on the nights of August 4 and September 14 and 15, 2000, yielded SI values of* 0.23 ± 0.04, 0.32 ± 0.01, *and* 0.49 ± 0.18, *respectively, where the reduction was attributed to aperture averaging. The probability distribution functions of the received signal at either end, mitigated by multi-beam averaging in one direction and by aperture averaging in the other direction, displayed lognormal behavior. Consequently, the measured fade statistics showed good agreement with a lognormal model.*

I. Introduction

Free-space optical communications technology is being developed at JPL to service an expanding set of future NASA missions. Higher data rates with a reduction in mass, volume, and power are key improvements spurring the technology development. Furthermore, significant bandwidth expansion in an unregulated portion of the electromagnetic spectrum with the potential for providing communications with a low probability of detection/interception is an added benefit. As a part of early end-to-end systems-level evaluation of free-space optical communications technology, mountain-top-to-mountain-top horizontal-path optical link demonstrations were initiated in 1998 [1,2]. As a result of these efforts, com-

[1] Communications Systems and Research Section.

The research described in this publication was carried out by the Jet Propulsion Laboratory, California Institute of Technology, under a contract with the National Aeronautics and Space Administration.

parisons between theory and observations of atmospheric turbulence-induced effects were made. With a few exceptions, the preliminary findings were favorable. An important area identified for further validation and testing was further characterization of the scintillation reduction due to multi-beam and aperture averaging. With these primary objectives, a follow-on ground-to-ground demonstration [3] was conducted during the summer of 2000. The results of this campaign are reported.

The optical link to be described was established between Strawberry Peak (SP), Lake Arrowhead, California, and JPL's Table Mountain Facility (TMF) in Wrightwood, California, spanning a 46-km near-horizontal path. The Optical Communications Demonstrator (OCD), a 0.1-m-diameter-aperture laboratory prototype terminal was located at SP. From this location, the OCD is blind pointed toward TMF, where a 0.6-m-diameter-aperture telescope serves as the receiving station. In order to provide a pointing reference to the OCD, the receiving station broadcasts a beacon to SP. A pair of 8.5-cm-diameter spotting telescopes retrofitted with avalanche photodiodes were co-located with the OCD and were used to monitor the beacon.

Investigations carried out, including the primary objectives mentioned above, are as follows:

(1) Validation of predicted link budgets

(2) Comparison of measured and theoretical scintillation indices

(3) Characterization of the reduction in the scintillation index with multiple beams

(4) Characterization of the fade statistics of the optical signal caused by atmospheric turbulence

Section II briefly discusses underlying theoretical channel effects that impact optical communications system performance. The operational details and link configuration are presented in Section III. Results, including comparisons with theoretical predictions, are described in Section IV, followed by conclusions in Section V.

II. Theory

Extensive theory [4–6] covering the phenomena of optical scintillation relevant to laser beam propagation, supported by a fair amount of experimental validation over horizontal [2,7] and space-to-ground [8–12] links, has been reported in the literature. The scintillation index (SI), σ_I^2, is defined as

$$\sigma_I^2 = \frac{\langle I^2 \rangle}{\langle I \rangle^2} - 1 \tag{1}$$

where $\langle\ \rangle$ refers to ensemble average and I represents irradiance. Furthermore, for optical beam waves, the SI is proportional to the Rytov variance, σ_R^2, defined as

$$\sigma_R^2 = 1.23 C_n^2 k^{7/6} L^{11/6} \tag{2}$$

where L is the path length, $k = (2\pi/\lambda)$, λ is the laser wavelength, and C_n^2 is the atmospheric structure function. The Rytov variance represents the SI of an unbounded plane wave in the "weak" fluctuation regime ($\sigma_I^2 < 0.6$). A heuristic model [13] was used to determine the dependence of σ_I^2 on σ_R^2. This theory is useful for predicting SI under moderate-to-strong irradiance fluctuations. The basic premise of the heuristic model is to view the random phase fluctuations of a propagating beam as having two independent contributions, namely, a small scale (diffractive) and a large scale (refractive) contribution. Of specific interest to our work is the situation where the inner scale, l_o, of the atmosphere is smaller than the Fresnel zone $\sqrt{(L/k)}$. For the range and laser wavelengths we are using, the Fresnel zone length is ∼75 mm, and the inner scale l_o typically is on the order of 1 to 10 mm.

The theoretical prediction of σ_I^2 relates to the SI as determined using a "point detector," defined as having a diameter smaller than the coherence length of the atmosphere. As the collection aperture is increased, spatial or aperture averaging [14] over the speckle intensity distribution reduces the fluctuations. The aperture averaging factor, A, is defined as the ratio of SI measured through a collection aperture of diameter D versus that for a point detector. For the 0.6-m-diameter aperture, taking into account the effect of the obscuration and receiving 852-nm laser light over a 46.8-km path, A is 0.11, whereas for a 9- to 10-cm aperture receiving 780-nm laser light, $A \sim 0.96$. The predicted theoretical bounds for σ_I^2 are significantly mitigated by having a 0.6-m receiving aperture, whereas the smaller diameter apertures ($\sim$10 cm) typical for planned low Earth-orbiting (LEO) and airborne terminals provide a negligible reduction in SI.

One method for reducing scintillation effects when using limited-diameter receiving apertures is the use of multiple beams. Non-coherent averaging of co-propagating multiple beams, with each beam traversing a slightly different atmospheric path, results in a reduction of the SI. A number of investigations of multi-beam averaging have been reported. While a discussion of the results observed will be postponed until Section IV, the predictions made are discussed briefly. Multi-beam averaging was used for the uplink beacon broadcast to the Engineering Test Satellite (ETS-VI) during the geostationary orbit laser communications demonstration (GOLD) [10,11]. Numerical simulations averaging N lognormal irradiance distributions indicated a reduction of $1/N$ for SI and a corresponding $1/\sqrt{N}$ reduction in standard deviation assuming identical mean irradiance values for each beam and also assuming that each beam displayed a lognormal intensity dependence. A report on a multi-beam demonstration [15] performed at the Massachusetts Institute of Technology (MIT) Lincoln Laboratories investigated the intensity variance for 1, 4, and 9 mutually incoherent argon laser beams. Here the predicted reduction in intensity variance is presented as a function of the Rytov variance. The predicted result suggests that the reduction achieved depends upon the severity of the atmospheric turbulence. In other words, as the Rytov variance increases, the scintillation index reduction factor, due to averaging of nine identical co-propagating beams, also increases. The range of Rytov variances covered by the simulation is 0 to 0.8. Finally, multi-beam averaging studies reported by AstroTerra Corporation [16] utilized the convolution integral of N transmitters, where scintillation was assumed severe enough to merit being represented by a decaying exponential. Here too the analytical expression showed that the reduction in SI scaled as the number of beams.

The statistical distribution of the received signal from a laser beam traversing an atmospheric path can be reasonably well represented by a lognormal distribution for SI values $<$0.6. A number of statistical distribution models for the intermediate range of SI values have been reported; however, as the SI approaches the so-called saturation range, the distribution evolves into a decaying exponential [17]. Provided the SI can be restricted to values less than 0.6 using the mitigation strategies discussed above, a lognormal model can be used to determine the fade statistics. For space-to-ground links, the lognormal probability distribution function (PDF) is convolved with spacecraft jitter in order to properly account for the intensity fluctuations [18].

For a lognormal distribution, the probability of a fade below a threshold level, P_{miss}, is given by [4]

$$P_{\text{miss}}\left(\sigma_I^2\right) = \frac{1}{2}\left[1 + \text{erf}\left[\frac{\frac{\sigma_I^2(r,L)}{2} + \frac{2r^2}{W_e^2} - 0.23 \times F_T}{\sqrt{2}\sigma_I(r,L)}\right]\right] \tag{3}$$

where F_T represents the dB value below the mean irradiance, r represents the mispointing with respect to the beam axis, and W_e represents the effective beamwidth at the receiver; $\sigma_I^2(r,L)$ represents the scintillation index measured for a path length of L and a distance r from the beam axis. The mean number of fades per unit time is given by the relationship [7]

$$\text{mean\_fades} = \nu_0 \exp\left\{ -\frac{\left[0.5 \times \sigma_I^2 + \dfrac{2r^2}{W_e} - 0.23 F_T\right]^2}{2\sigma_I^2} \right\} \tag{4}$$

where ν_0, known as the quasi-frequency, represents the width of the normalized irradiance power spectrum, $S(\omega)$, as indicated by the following relation [4]:

$$\nu_0 = \frac{1}{2\pi} \left[\frac{\int_0^\infty \omega^2 S(\omega) d\omega}{\int_0^\infty S(\omega) d\omega} \right]^{1/2} \tag{5}$$

with ω being the angular frequency of the temporal irradiance fluctuations. The mean fade duration is the ratio of the fade probability to the mean number of fades. Thus, knowing $\sigma_I^2(r, L)$ and $S(\omega)$ from measurements, the fade statistics of a beam can be predicted using Eqs. (3) through (5).

III. Operations and Setup

A. Operational Scenario

Figure 1 shows a sectional view of the intervening terrain along the 46-km link. The optical path, approximately 2 km above sea level, should provide relatively favorable atmospheric turbulence as evidenced by numerous measurements and models. The optical link was initiated by broadcasting a multi-beam beacon comprised of eight co-propagating lasers (780-nm continuous wave) from the 0.6-m-aperture telescope at TMF to SP. The OCD located at SP received the beacon and, using it as a pointing reference, retransmitted a communications signal at 852 nm. A sturdy tripod was used for mounting the OCD.The upgraded OCD (Subsection III.C) control system was not equipped with coarse-pointing electronic control; thus, manual adjustment of the azimuth elevation mount was used to acquire the beacon.

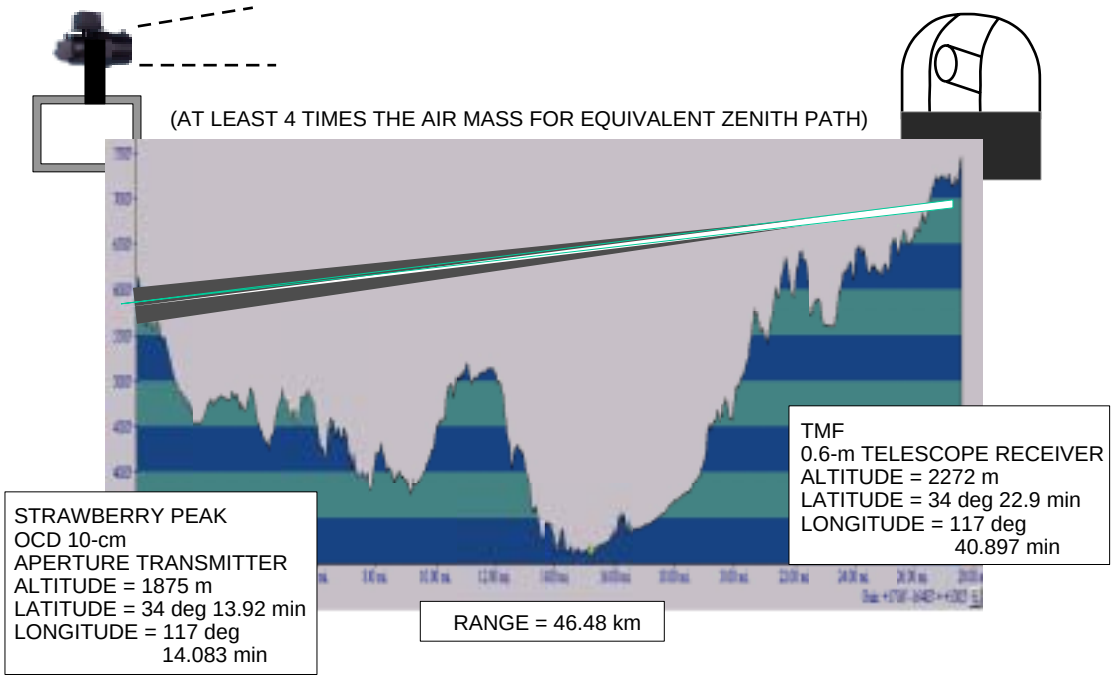

Fig. 1. Sectional view of the intervening terrain between TMF and SP.

Prior knowledge of the 0.6-m Ritchey–Chretien TMF telescope settings—hour angle (HA) and declination (DEC)—is used to point toward SP. Under nighttime conditions used throughout our demonstration, the pointing is easily validated with the aid of an intensified charge-coupled device (CCD) camera display monitor attached to the co-bore-sighted spotting telescope (0.15-m aperture). Once the 0.6-m telescope is pointed to SP, the multi-beam beacon comprised of 8 co-aligned beams (see Subsection III.B for details) is broadcast from TMF to SP.

Acquiring the beacon in the OCD's relatively narrow ∼1-mrad field of view (FOV) required careful manual adjustment. To ease this process, the 852-nm communications laser beam transmitted by the OCD was monitored through the intensified camera video monitor as the OCD was manually adjusted to point toward TMF. Once this 852-nm laser spot was sensed at TMF, it was relatively easy to guide the manual adjustments of the OCD coarse azimuth and elevation mount in order to "walk the beam in." Prior to excessive saturation of the intensified camera, hand off to a power-meter sensor located at the Coudé focus of the 0.6-m telescope was possible. The power received at the TMF was increased by further coarse adjustments of the OCD at SP. Finally, the OCD fine-steering mirrors were electronically stepped to maximize the power received at TMF. The latter automatically resulted in acquisition and centering of the beacon spot on the OCD's tracking sensor.

A pair of 8.5-cm-diameter Maksutov–Cassegrain spotting telescopes, retrofitted with avalanche photodiodes (APDs) in their focal plane and mounted on separate tripods, were also used to receive the beacon. The beacon footprint at SP was typically ∼4 to 7 m in radius so that the spotting scopes could be mounted within a few meters of the OCD. The alignment in this case was accomplished by first sending a helium neon (He:Ne) laser through the TMF telescope nominally co-aligned to the outgoing beacon. This eye-safe He:Ne laser aided the coarse alignment of the spotting telescopes, followed by finer alignment to maximize the 780-nm signal sensed by the APD detectors.

All the laser beams transmitted through the atmosphere were at irradiance levels well below the maximum permissible exposure (MPE) levels at the exit apertures specified by the American National Standards Institute (ANSI) Z-36.1 eye-safety standards.

B. Experimental Setup at the Table Mountain Facility

A 0.6-m telescope at TMF was used for broadcasting the beacon (780 nm) as well as for receiving the communications signal (852 nm). The telescope's Coudé configuration was used with a transmit–receive optical assembly located in the Coudé room.

Figure 2 shows a schematic representation of the multi-beam beacon laser assembly. The laser sources used were four thermoelectrically cooled (TEC) fiber-coupled laser diodes [62.5-μm core diameter; 0.25 numerical aperture (NA)] emitting approximately 25 mW each at 780 nm. The output of each laser was split using a 50/50 multi-mode fiber splitter and then collimated. The resulting eight collimated beams were co-aligned in a ring pattern using the prism assembly. The co-propagating beams were then steered through a lens assembly chosen to match the telescope optical train and deliver the required beam divergence. This resulted in all eight beams uniformly diverging from the Coudé focus and incident in an annular pattern on the 0.6-m telescope primary mirror. A photograph of the eight-beam pattern projected on the telescope dome is also shown in Fig. 2. The lens assembly was designed to provide spots with a 100 percent energy diameter of 4.1 cm on the primary mirror, corresponding to a nominal 120-μrad divergence per beam. The design was based on estimated beam profiles emitted from the fiber core of the lasers. Difficulty in modeling the actual beam profile emerging from multi-mode fibers introduces uncertainty in the realized beam divergences. The beams could be attenuated individually or in any desired combination by means of a neutral density (ND) filter wheel (not shown). Typically, ND filters with indices of 1.7 to 2.6 were used when transmitting all eight beams, resulting in 100- to 500-μW of beam power exiting the TMF telescope. The poorly defined beam profiles exiting the multi-mode fibers

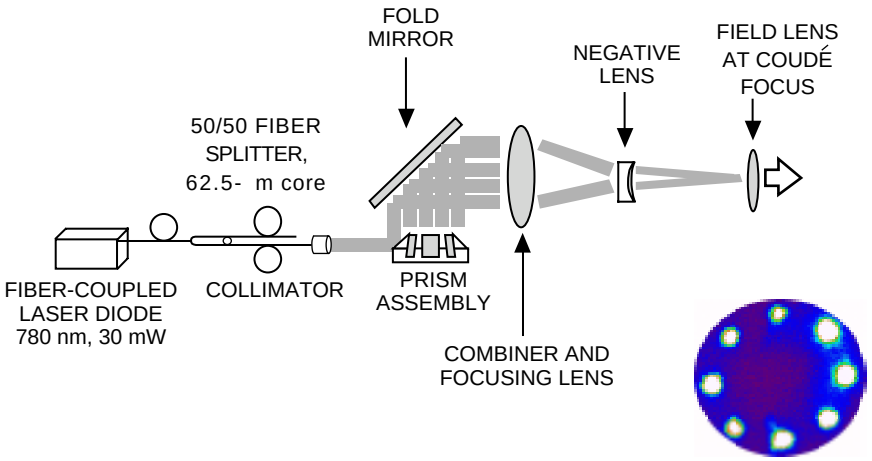

Fig. 2. Schematic of the multi-beam beacon assembly used to broadcast eight 780-nm laser beams to SP. A captured video image of the appearance of the beacon laser spots on the telescope dome inner wall is shown in the lower right.

were recorded by having a 90/10 pellicle beam splitter inserted after the negative lens (not shown in Fig. 2), and displaying the focused laser spot on a CCD camera connected to a frame grabber (not shown in Fig. 2).

Figure 3 shows a schematic of the overall transmit–receive optical train used in the TMF telescope Coudé room. The relative configuration of the beacon assembly is apparent. A dichroic beam splitter separates the transmit–receive optical paths. The received 852-nm signal is transmitted through the dichroic beam splitter and re-collimated. The collimated beam optionally can be split among three receiving channels by manipulating the flip-mounted (curved arrow) beam splitter shown in Fig. 3. The three receiving channels are for data, focal spot monitoring, and pupil image of the telescope primary mirror.

A power meter was used near the Coudé focus for measuring received power. Irradiance fluctuations also were measured at the same location using a photodiode (4×4 mm square), sampled at 2.5 kHz by a digitizing oscilloscope. Finally, Fig. 3 also shows the He:Ne laser used for establishing the telescope bore sight as well as for transmitting to SP. Note that unlike the beacon the He:Ne beam is transmitted without any optical conditioning so that it exits the telescope with essentially the same divergence as the laser. This was measured to be approximately 800 μrad. Other TMF setup details related to data acquisition are identical to the descriptions provided in [1] and [2].

C. Experimental Setup at Strawberry Peak

The SP setup is shown in Fig. 4. An 852-nm optical-fiber pigtailed diode capable of high-speed (500 Mb/s) on–off keyed modulation provides ~8 mW of average optical power to the OCD. Approximately 3 to 4 mW of optical power exits the telescope.

The auxiliary beacon-monitoring spotting telescopes (Meade ETX 90EC) were retrofitted with avalanche photodiodes (Hamamatsu Model C5460-1) to record the incoming beacon irradiance fluctuations. Laboratory characterization of these 3-mm-diameter APDs indicated a dynamic range of 37 to 38 dB. Furthermore, the APDs also were calibrated so that the measured signal could be converted into optical power. Data sets obtained using the spotting telescope/APD assembly consisted of digitized sequences of received laser signal recorded for 20-s durations, while sampling at 2 to 2.5 kHz. The additive contribution of noise due to electronics (detector, amplifier, and read-out) and background was accounted for by determining average threshold levels in the absence of incident signal. The average

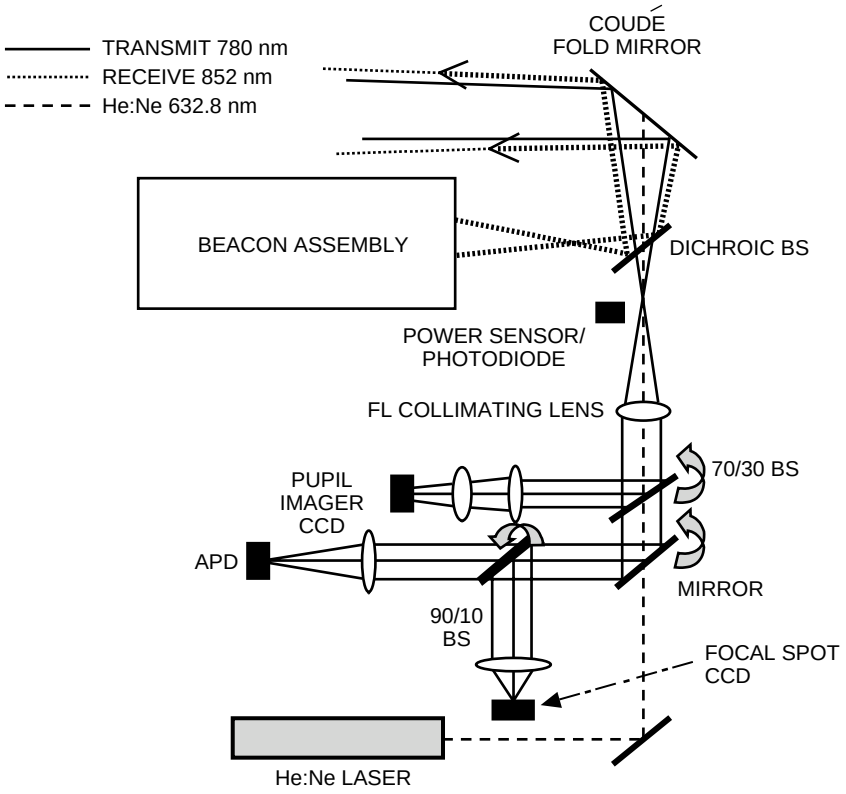

Fig. 3. Overall Coudé room assembly used at TMF; the details of the receive train are shown with the beacon (transmit) assembly detailed in Fig. 2.

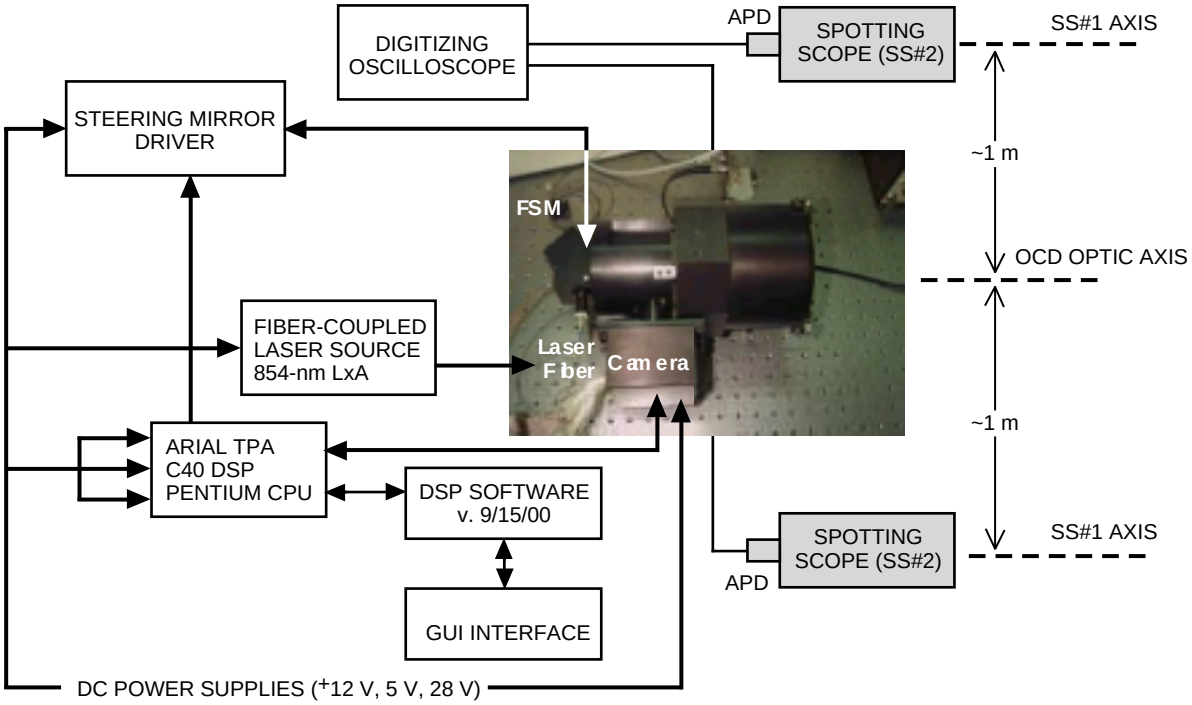

Fig. 4. Block diagram of the SP setup used during the optical link demonstration.

and standard deviations of acquired signals that exceeded the threshold were used to infer the scintillation index. Additionally, threshold discrimination allowed the estimation of fractional fades, while dynamic range was evaluated from the recorded maximum and minimum signals above threshold. Histograms of threshold-discriminated APD signals were fitted to a lognormal function, using a polynomial [11] method. Finally, the irradiance temporal spectra, determined using fast-Fourier transformation (FFT), were used for determining ν_0 [Eq. (5)], the quasi-frequency of the irradiance power spectrum.

IV. Results and Discussion

In this section, the observations recorded during the optical link demonstration are reported. Wherever appropriate, comparisons are made with existing theoretical models as well as previously reported work.

A. Link Analysis Validation

1. TMF to SP. Link budgets were predicted for a single-beacon laser beam propagating from TMF to SP and incident upon the receiving aperture of a spotting telescope located at SP. Reasonable estimates for relay optical efficiencies and atmospheric attenuation were made.

The prescribed beacon divergence of 120-μrad (see Subsection III.B) assumed uniform illumination of the multi-mode fiber core (62.5-μm diameter). In reality, the intensity pattern at each of the fiber cores consisted of numerous randomly distributed "hot spots." Far-field intensity distributions of individual beacon beams arriving at SP were measured. This was achieved by stepping the TMF 0.6-m telescope, first in hour angle (HA) with fixed declination (DEC), and then in DEC with fixed HA, while recording average received power through a pair of spotting telescopes at SP. Two of the eight lasers were scanned on June 28, 2000, followed by two more scans on June 29, 2000. Figure 5(a) shows the intensity distribution resulting from one such line scan. The pair of lines (dashed and solid) corresponds to simultaneous measurements made through two spatially displaced telescopes (see Fig. 4). Note that the APD output voltage is recorded as a negative quantity in Fig. 5(a). For comparison, the beam point spread function (PSF) recorded by a CCD camera prior to being launched from TMF is shown in Fig. 5(b). The data set displayed in Fig. 5 is representative of all four beams characterized. Although a one-to-one correspondence between the PSF prior to launch and the intensity distribution after traversing 45 km of atmosphere cannot be concluded from comparisons of Figs. 5(a) and 5(b), they provide strong evidence that features of the PSF are retained as the beam propagates the atmospheric path. The measured far-field beacon profiles at

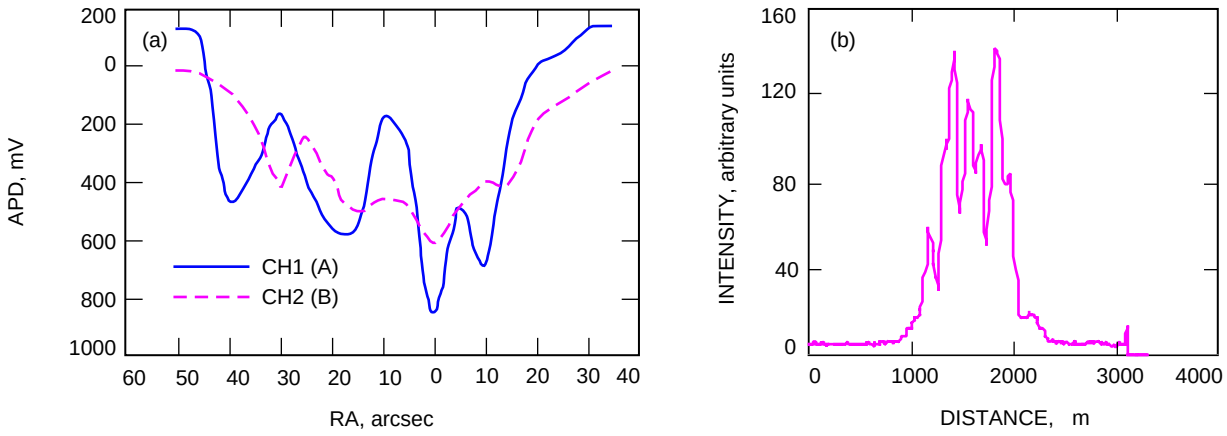

Fig. 5. Scan from June 29, 2000: (a) the intensity distribution recorded by a pair of spotting telescopes at SP during an HA scan of the TMF telescope while broadcasting the beacon beam and (b) the PSF of the same beacon beam recorded at the TMF prior to launch. Although the comparison of (a) and (b) does not allow a one-to-one comparison, it provides strong evidence that features present in the intensity profile are preserved after propagating 45 km through the atmosphere.

SP were transformed from HA and DEC to azimuth and elevation angular widths at SP using standard co-ordinate transformation equations [20]. Table 1 summarizes the results. The beam footprints are elliptical with aspect ratios of 0.7 to 0.9. The full widths (100 percent energy) of the beams measure 160 to 340 μrad, compared to a design goal of 120 μrad. The increased beam divergence observed is consistent with the smaller effective beam diameters emitted from the multi-mode fibers. Using the numbers reported in Table 1, the inferred beam footprints range nominally from 7.5 to 16 m. Using these values, the best-, nominal-, and worst-case link budget predictions shown in Table 2 were made.

The received power reported in Table 2 was determined by converting the APD voltage to power based upon prior laboratory calibration. The system loss in Table 2 represents the cumulative effect of transmission losses experienced due to relay optics efficiencies at the transmitter and receiver, as well as to the space loss. Full-width beam divergences of 160, 250, and 340 μrad were used for the best, nominal, and worst cases. The atmospheric attenuation was assumed to be 3, 4, and 5 dB for the best, nominal, and worst cases. A 3-dB pointing loss was assumed for the worst case while zero pointing losses were allocated to the best and nominal cases. Figure 6 shows the distribution of the received powers in dBm measured at SP for transmission of single-beacon beams. The dashed lines in Fig. 6 represent the predicted best, nominal, and worst cases obtained from Table 2. The dominant variable causing the spread in predicted bounds of received power is the beam divergence. The measured distribution shows that at least 75 percent of measured powers are confined within a 6- to 8-dB spread. A closer examination of the data reveals that half the single-beam received power measurements on the first 2 days contributed to the lower received power values, whereas on the third and final day all measurements fell within the 6- to 8-dB spread. Furthermore, the third day's measurement represents received power made through the pair of spotting telescopes as opposed to the first 2 days, when only one spotting telescope was used. The significance of these observations is that beam divergences are closer to the 150- to 250-μrad range and that with good alignment the total spread in received power can be confined to within a spread of 6 to 8 dB. The lower received powers shown in the distribution of Fig. 6 were most probably due to a large mispointing bias.

Table 1. Summary of the full-width at half maximum beamwidths measured in HA and DEC and transformed to elevation and cross-elevation angular width.

Beam 1		Beam 5		Beam 3	
EL, μrad	AZ, μrad	EL, μrad	AZ, μrad	EL, μrad	AZ, μrad
138	153	128	171	93	83

Table 2. Link analysis for transmission of a single beacon laser from TMF to SP.

Link parameter	Best case, dB	Nominal case, dB	Worst case, dB
Transmitted power	11.46	11.46	11.13
System loss	−48.16	−53.16	−60.33
Atmospheric loss	−3.0	−4.0	−5.0
Pointing loss	0	0	−3.0
Net received power	−39.7	−45.7	−57.2

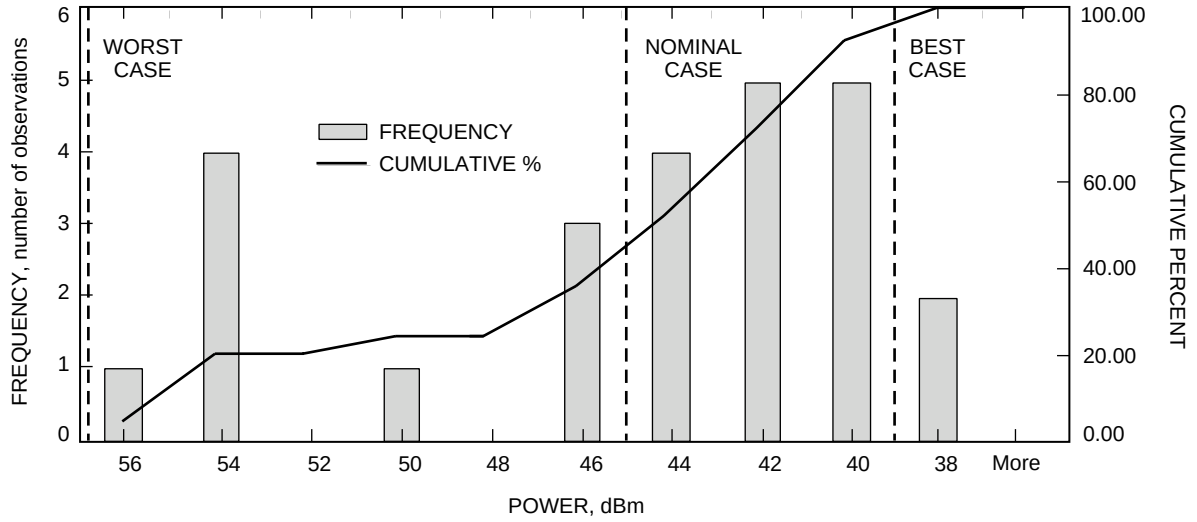

Fig. 6. Distribution of measured powers relative to the best-, nominal-, and worst-case predictions (dashed lines).

As a final test, the received He:Ne power at SP was measured. Using a He:Ne beam divergence of ∼800 μrad (measured over a long laboratory path) and assuming the relay optics losses and atmospheric transmission are the same as in Table 2, the predicted average received power was −58.8 dBm versus measurements ranging between −58.9 to −58.3 dBm.

2. SP to TMF. The OCD beam divergence observed in the laboratory using Lasercom Test and Evaluation Station (LTES) prior to the ground-to-ground campaign was 22×17 μrad, in agreement with previous measurements [21]. The beam footprint received from SP can be manipulated with the fine-steering mirror so that instead of being incident on the telescope aperture it is deliberately off-pointed on the TMF telescope-building wall. By doing so, the beam footprint arriving at TMF can be visually examined through an infrared (IR) viewer. Using this technique, the size of the beam footprint received at TMF was estimated to be approximately 2.1×1.88 m, compared to an expected size of 1×0.8 m. The increase in footprint size is attributed to atmospheric beam spreading.

Table 3 shows the link analysis for the OCD laser transmitted from SP to TMF. The transmitted power shown in Table 3 was measured at the end of the optical fiber that couples light into the OCD optics. The net system-loss results after optical transmission and space losses were added to antenna gains at the transmitter (OCD) and receiver (0.6-m TMF telescope). All of these quantities are known within ∼1 dB of uncertainty. Atmospheric transmission at zenith for 780 and 852 nm differs [22] by ∼1 percent, so for the purposes of our link analysis they have been assumed to be identical. The best-case pointing loss is neglected, assuming perfect on-axis pointing, whereas for the nominal and worst cases, 3 and 28 dB are used. The large worst-case pointing loss is included based upon an assumed mispointing bias that results in the third lobe of a far-field Airy pattern being incident upon the telescope. Theoretically, the third Airy lobe or ring is down in intensity by 28 dB and spatially 3 times the radius of the first ring away from the beam center [23].

Figure 7 shows a distribution of the power measurements made at the Coudé focus of the TMF telescope using a calibrated power meter, with the dashed lines representing the link analysis results from Table 3. The agreement is very good. The single-power measurement of −40.3 dB supports the use of a 28-dB worst-case pointing loss. This data point was obtained by starting with the OCD aligned optimally and then stepping the fine-steering mirrors (34 μrad in one axis and 5 μrad in the second axis), and it corresponds to approximately 3 times the first bright ring radius of 11 μrad. Moreover, visual examination of the spot provided an estimated 3.6-m displacement of the spot from the telescope axis

Table 3. Link analysis for OCD laser transmission from SP to TMF.

Link parameter	Best case, dB	Nominal case, dB	Worst case, dB
Transmitted power	8.45	8.45	8.45
System loss	−12.96	−13.32	−14.01
Atmospheric loss	−3.0	−4.0	−5.0
Beam-spread loss	−2.22	−3.12	−4.12
Pointing loss	0	−3.01	−28
Net received power	−9.73	−15	−42.68

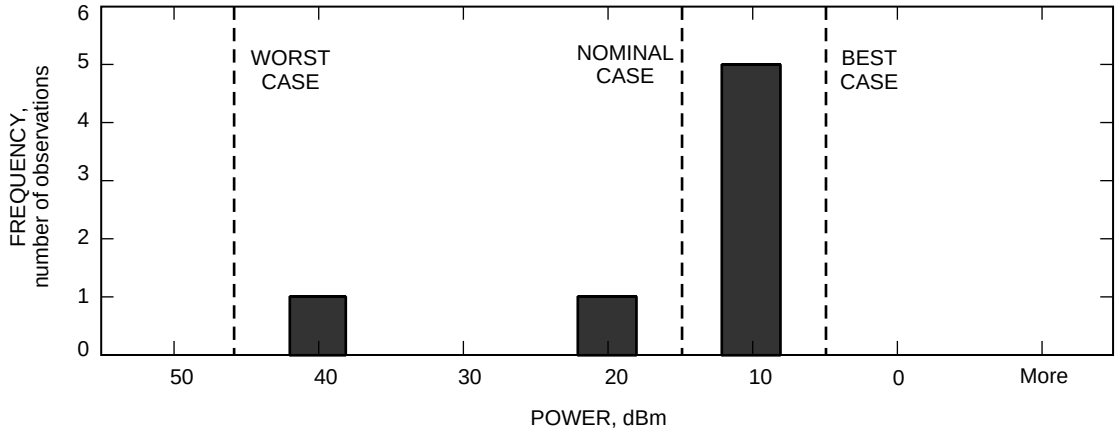

Fig. 7. Representation of the predicted best-, nominal-, and worst-case link uncertainties and the distribution of measured powers; note that the single 40 dBm measurement was obtained by deliberately off-pointing the OCD beam.

that is close to 3 times the observed spot radius. The variations in received power observed at TMF are attributed to mispointing bias losses, since the beam divergence of the single-mode laser exiting the OCD is well-known.

B. Scintillation Characteristics

1. Theoretical Predictions. The theoretical dependence of the scintillation index, σ_I^2, on the Rytov variance, σ_R^2, discussed in Section II is plotted in Fig. 8. The scintillation-index level corresponding to the onset of saturation increases as the atmospheric inner scale value, l_o, is increased from 1 to 10 mm. The predicted results are for plane and spherical waves; the characteristics of the Gaussian beam profiles are expected to fall between the spherical- and plane-wave models.

The Air Force Geophysical Laboratory (AFGL) CLEAR I Night model [8] can be used to obtain C_n^2 corresponding to the altitudes of TMF and SP (see Fig. 1). Table 4 shows these values. The corresponding range of Rytov variances derived using Eq. (2) and scintillation-index (SI or σ_I^2) bounds determined from Fig. 8 are tabulated. These theoretical bounds are compared to measured SI values on single beams (Subsection IV.B.2).

Note that the strategy employed in our demonstration is to mitigate the severe atmospheric turbulence and resulting high SI and unfavorable fade statistics by using multi-beam averaging for the beacon being

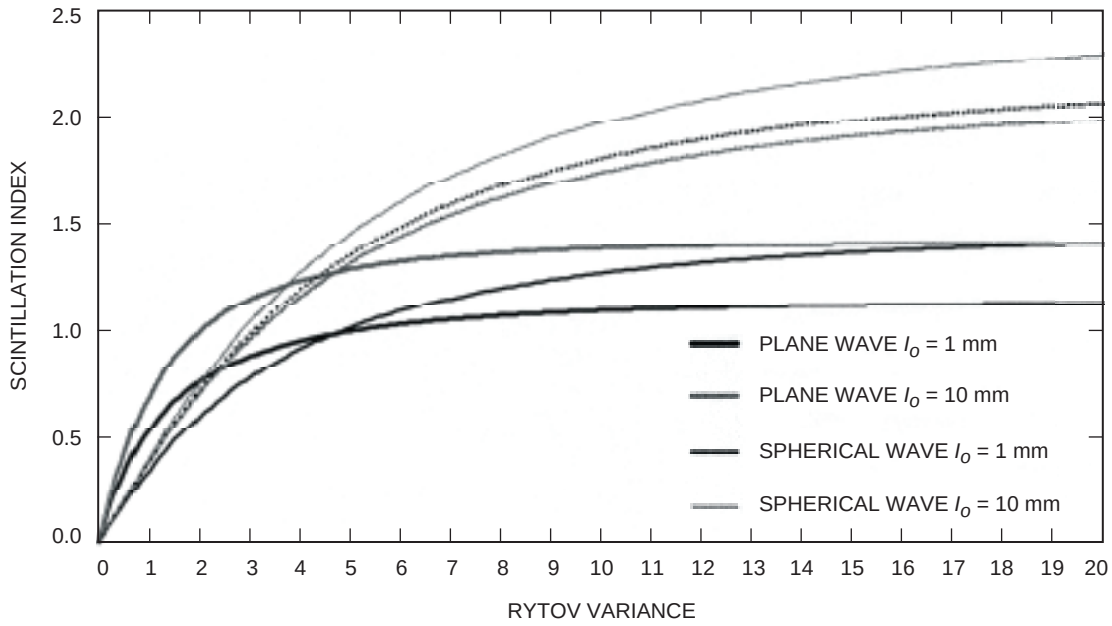

Fig. 8. The theoretical dependence of the scintillation index (normalized variance of irradiance) on the Rytov variance. The dashed lines represent the region in agreement with measurements (see Subsection IV.B.2).

Table 4. Some predicted values of the Rytov variance, σ_R^2, and scintillation index, σ_I^2.

Beam path	C_n^2	σ_R^2	σ_I^2			
			$l_o = 1$ mm		$l_o = 10$ mm	
			Plane wave	Spherical wave	Plane wave	Spherical wave
TMF to SP, 780 nm	5.2×10^{-17} to 10^{-16}	2.7 to 5.1	0.85	0.70	1.10	0.95
			1.00	1.00	1.30	1.470
SP to TMF, 852 nm	5.2×10^{-17} to 10^{-16}	2.4 to 4.6	1.055	0.831	1.07	0.888
			1.191	1.239	1.265	1.383

received by relatively small-aperture telescopes at SP and by relying upon aperture averaging resulting from use of the 60-cm-diameter aperture for the beam received at TMF.

2. Results. Scintillation index measurements of 1, 2, 4, 6, and 8 co-propagating laser beams were performed. These measurements were made on the nights of June 27 through 30, 2000. The SI was obtained from the measured mean and standard deviation of the signal received through the spotting telescopes and recorded on a digitizing oscilloscope. Subsequently, the SI of the combined eight-beam beacon was monitored on the nights of August 3 and September 14 and 15, using both the spotting telescopes and a fast framing (1-kHz) CCD tracking sensor on the OCD. The results obtained with the CCD will be discussed in a future article, while the APD results are discussed below.

Single-Beam Results: Single 780-nm Beam Transmitted from TMF to SP. The results from processing the data obtained during the nights of June 28 through June 30 are presented in Table A-1 of the

Appendix. For single beams, SI values range from 0.9 to 1.4, 1.2 to 1.99, and 0.8 to 1.62, respectively, for the 3 nights (in Table A-1, beam 4 on June 28, 2000, is discarded as unreliable because of the low average signal level with very high fractional fade). The measured SIs exceed the theoretically predicted plane-wave saturation levels shown in Fig. 8 but are bounded by the value shown for spherical waves. However, to reconcile spherical-wave theory with the range of measured SI, either l_o and/or Rytov variance must cover a wide range of values. Atmospheric inner scale, l_o, variations reported [24] in the literature typically are ± 0.5 mm for mean values ranging from 1 to 10 mm. On the other hand, an order of magnitude fluctuation in C_n^2 measurements has been reported [25] for 10-min averaged values over 100- to 300-m paths. Given the much longer atmospheric path length and measurement duration, similar variations of C_n^2 cannot be ruled out. Allowing C_n^2 to span a range that results in Rytov variances of 2 to 17, for example, would yield a theoretical curve with the atmospheric inner scale, l_o, between 1 and 10 mm along which our SI measurements would fall, shown approximately by dotted lines in Fig. 8. The beams used can be best represented by a Gaussian profile and, as expected, the SI values fall somewhere between the plane- and spherical-wave models. In our situation, a further complication is posed by the multi-mode nature of the launched laser beam (see Fig. 5). The quasi-quantitative agreement of measured SI with the heuristic model is encouraging, although a more rigorous and desirable test would be to concurrently monitor C_n^2 and l_o independently at either end of the link. The higher SI values on June 28, as compared with June 27 and June 29, were compared to wind speeds monitored by the atmospheric visibility monitoring (AVM) station at TMF, but no correlation was established.

In the previous campaign conducted in 1998, SI values ranging between 0.7 and 1.03 consistent with the above results were reported. The 1998 campaign results produced a limited data set acquired on a single night over a shorter time period. Moreover, the detector used in the previous campaign was a p-type-intrinsic-n-type semiconductor (p-i-n) photodiode rather than an APD. This is noteworthy because, while the p-i-n detector does not have the sensitivity and dynamic range of the APD, it also is not affected by excess noise associated with the APD detector.

We compared measurements reported by other workers [7] over a 150-km horizontal path to the theoretical model. Taking into account the aperture-averaging factor, these measurements yield a σ_I^2 value of $\sim$1.00 for a σ_R^2 value of 3.31. These measurements fall in a region of the theoretical curves (Fig. 8) where the plane- and spherical-wave theories overlap; therefore, the match between experiment and theory leaves the issue of plane- versus spherical-wave models ambiguous. The time span over which the cited measurements were carried out is not reported. Therefore, whether the narrow Rytov variance range reported applies to a limited set of observations or a long time period is not clear.

Histograms of the single-beam signal levels displayed reasonable fits to the lognormal function, with correlation coefficients $\geq$0.95. However, the derived SI based upon fitted lognormal parameters is higher than the empirical values by as much as a factor of 2. A more rigorous test comparing the higher-order (third-, fourth-, and fifth-order) moments to an ideal lognormal distribution [4] also revealed significant deviations between measurement and theory.

Single-Beam Results: OCD 852-nm Beam Received at TMF. The single-beam scintillation measured on the communications laser (852 nm) transmitted by the OCD and received at TMF is aperture averaged through the 60-cm telescope. Theory predicts a scintillation index reduction by a factor of 0.22. Consistent with Table 4, the SI range corresponding to the Rytov variance (see dotted lines in Fig. 8) is $\sim$0.81 to 1.5. Allowing for the aperture-averaging factor, measured SI values should range from 0.18 to 0.3. As reported in Table A-2, the measurements recorded on August 4 and September 14 of 2000 display excellent agreement with this prediction. On September 15, 2000, the reported SI values in Table A-2 are higher. The September 15, 2000, data are clustered in a different region from the remaining data, consistent with the higher SI observed. The larger SI and fractional fade observed on September 15, 2000, can be attributed either to more severe atmospheric turbulence arising due to local meteorological conditions or to artifacts arising due to poorer alignment. If the former were true, the beacon scintillation measurements recorded at SP should also be affected, and they are (compare September 15, 2000, SI values in Tables A-2 and A-3) as reported in the following subsection.

Aperture-averaged [14] irradiance fluctuations monitored at TMF display good fits to lognormal distributions. The correlation coefficients are $\geq$0.95, and derived SI values are within 30 percent of the empirical values. In this case, a comparison of the higher-order (third-, fourth-, and fifth-order) moments showed good agreement. The lognormal statistics displayed by the aperture-averaged signal received at TMF allow for testing of the fade statistics utilizing a lognormal probability density function.

Figure 9(a) shows the theoretically expected probability of miss versus SI for 6-, 8-, 10-, and 12-dB fade depths as represented by Eq. (3). The fade depth is defined as the dB-level drop from the mean signal level. Note that r, the displacement from beam axis in Eq. (4), has been set to zero, i.e., mispointing effects on fade statistics are neglected. The probability of miss increases by less than a factor of 2 for an off-axis bias of 5 μrad for a 23-μrad full-beam divergence.

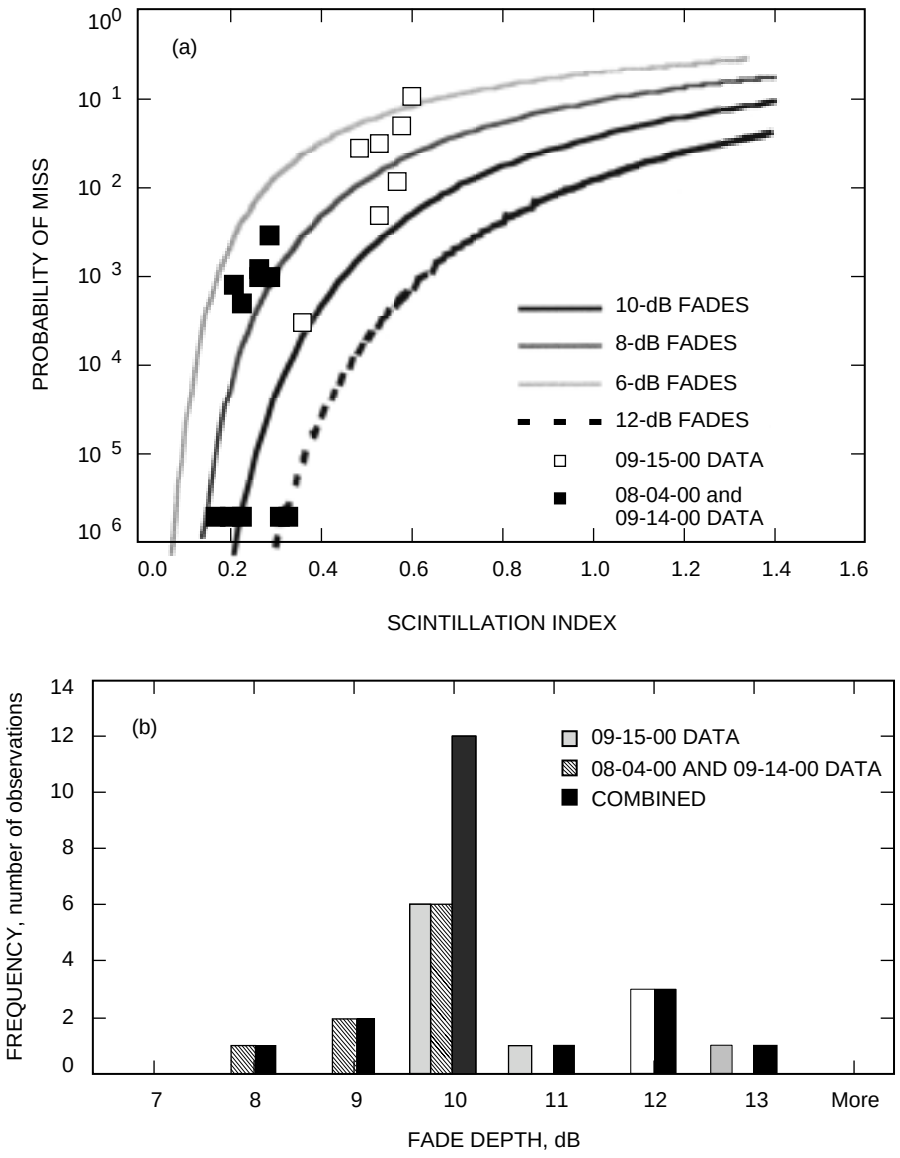

Fig. 9. Fade depth: (a) comparison of the measured and predicted lognormal fade statistics and (b) the distribution of the fade depths observed.

The fade threshold in our measurements is set by the noise plus background of the detector used (a p-i-n diode in this case). The magnitude of the mean signal received relative to the detector threshold determines the observed fade depths. Figure 9(b) shows a histogram of these empirical fade depths. The histogram shows three data sets, namely, the combination of data obtained on August 4, September 14, and September 15, the data for August 4 and September 14, and the observations made on September 15. Consequently, the measured SI versus the fractional fade is also plotted in Fig. 9(a), again making a distinction between the data for August 04 and September 14, 2000, and for September 15, 2000. The September 15, 2000, data are consistent with the higher SI values observed. Artifacts such as the quantization levels set by the 8-bit digitizing oscilloscope used to record the data plague comparison of empirical data with theoretical fade statistics. In spite of these artifacts, the measurements display a trend consistent with lognormal fade statistics within a margin of 2 dB.

Multiple-Beam Results. Figure 10 presents a graphical summary of SI values measured between June 28 and 30, including single beam (results discussed in the previous subsection) and various combinations thereof. A reduction in SI with an increasing number of co-propagating beams is observed on all three nights. An overall average reduction factor of 3, 3.2, and 3.7, respectively, was achieved for June 28, 29, and 30. The observed reduction in SI can be approximated reasonably by a $\sqrt{N}$ dependence, where N is the number of beams; however, an explanation for this dependence is not obvious. In previous analysis [10], the suggested reduction was modeled as the convolution of identical independently distributed lognormal distributions with the predicted reduction in SI scaling as the number of beams used. The single-beam PDFs derived from our measurements are clearly not identical. The mean received signal levels for the individual beams show variations that often far exceed the differences in launched power. These differences may arise from the receiving spotting telescope aperture being located in an intensity valley of one beam while being near the peak for a second beam (see the point spread functions of Fig. 5). Alternatively, misalignment between the beams may cause the difference. The two equally plausible explanations give rise to ambiguity in interpreting observed relative signal strengths. The data of June 28, 2000, show relative differences in signal strengths exceeding an order of magnitude (neglecting beam 4 for reasons mentioned earlier), while for June 29 the signal strength from all 8 beams is within an order of magnitude (see Table A-1). A numerical convolution of the 8 PDFs was performed and clearly did not agree with the PDF measured when the 8 beams were co-propagated. Furthermore, the lack of agreement persisted with data obtained on different nights and for subsets of 4 beams. The comparisons showed that the numerical convolution deviated from a lognormal PDF whereas the multi-beam measurements did not. In fact, the multi-beam measured PDFs yielded better fits to lognormal behavior as determined by a comparison of higher-order moments. The fact that the measured multi-beam PDF does not agree with

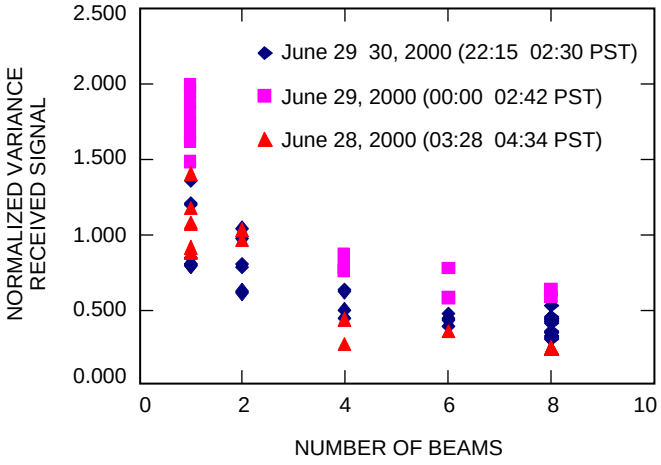

Fig. 10. Measured reduction of normalized variance or SI as a result of multi-beam averaging.

the convolution of the individual-beam PDFs strongly suggests that in addition to being non-identical the beam irradiance fluctuations are partially independent processes. The basis of cross-correlation can be argued by virtue of the fact that the beams overlap after traversing some distance. Once they overlap, the individual incoherent beams are subject to identical atmospheric refractive index perturbations. Thus, given beam divergence bounds of 160 to 340 μrad and beam separations ranging from ~20 cm (adjacent) to ~50 cm (diametrically opposite), adjacent beams will traverse 2.5 to 12.5 km prior to overlap while the farthest beams will traverse 6.5 to 32 km prior to overlap. The problem is further complicated by the multi-mode nature of the individual beams. Analysis to match the measured multi-beam PDF with the measured single-beam PDFs was not undertaken. It is also significant that the 8 beams combined display a lognormal PDF, whereas the central limit theorem would predict that the convolution of truly independent random processes would tend to a normal distribution.

In results reported elsewhere [15] for a 5.4-km range with 9 co-propagating argon laser beams, the predicted reduction was shown to depend on the severity of atmospheric turbulence or Rytov variance. The predictions reported indicate as much as a 10-fold reduction in SI for Rytov variances between 0.4 and 0.5 and a 3- to 4-fold reduction for a Rytov variance of 0.2. The data presented, while displaying large error bars in the measured normalized variance or SI, do agree with the predicted reduction. However, the authors claim only a 3-fold improvement in SI for the 9-beam beacon, suggestive of a $\sqrt{N}$ dependence. Unfortunately, the predictions presented here do not extend to the range of Rytov variances that was encountered during the optical link being discussed in the current article and shown in Fig. 8.

In other terrestrial link measurements [16], the predicted N-fold reduction in scintillation index for a 2.4-km path was confirmed; however, when the range was extended to 10.4 km, the extent of reduction was significantly reduced. A 4-fold reduction for 16 beams was reported. The lack of agreement with predictions was attributed to alignment uncertainties.

During the GOLD (ground-to-geostationary (GEO) satellite) experiment, the SI values reported were 0.12 for 2 beams and 0.045 for 4 beams. Based on numerical analysis, an SI value of 0.18 was inferred for a single beam, although this was not confirmed by measurement.

The reduction in SI using multiple beams shown in Fig. 10 was corroborated by similar measurements made first on August 4 and then again from September 13 through 15. During these measurements, the beacon irradiance was monitored simultaneously by the pair of spotting telescopes (with APD detectors) and the CCD sensor on the OCD. The irradiance of the multi-beam beacon was lowered, relative to the levels used from June 27 through 29, in order to prevent saturation of the CCD. This resulted in an order of magnitude lower received signal at SP as compared to data reported in Table A-1. The spotting telescope results are summarized in Table A-3 of the Appendix. Note that the SI values recorded on September 15, 2000, are higher than the data on other nights. This is consistent with higher SI values recorded at TMF for the counter-propagating communications laser beam, suggesting that local meteorological conditions on that night probably caused more severe irradiance fluctuations. The plots of Fig. 11, where the higher-order lognormal theoretical moments are compared, best summarizes the data. The abscissa in this plot represents $(\mathrm{SI}+1)$. The predominance of measured SI values ranging between 0.2 and 0.3 is noteworthy. The agreement with lognormal theory is very good for the multi-beam scintillation. Once again, as was shown for data received at TMF, the measured fade statistics can be compared with lognormal theory while realizing the dependence of the measured fractional fades are affected by the magnitude of the signal relative to the noise floor of the detector, as discussed in Subsection IV.B.2. The comparison is made using data obtained on the night of August 4 only. Figure 12(a) shows the theoretical curves along with the data points measured using two spotting telescopes designated as channels 1 and 2. The measured data points fall between the 6- and 8-dB fade-depth theoretical curves. The histograms of the fade depths for the two channels of data shown in Figs. 12(b) and 12(c) support this observation.

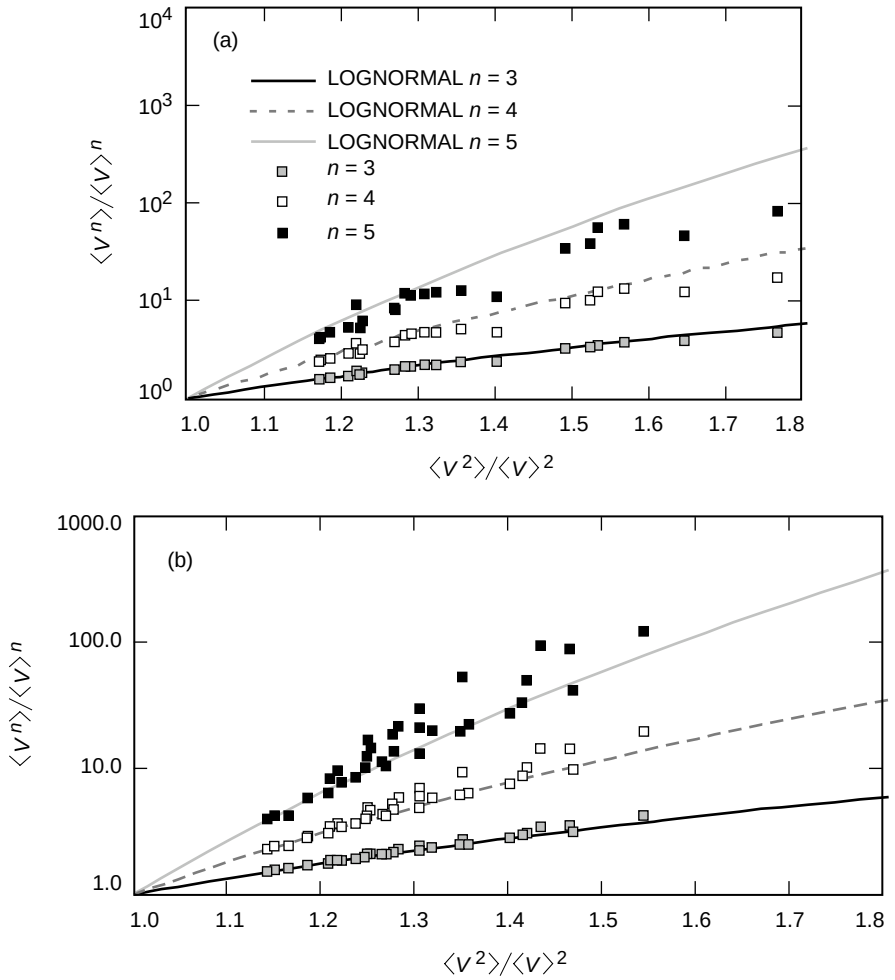

Fig. 11. Comparison of measured SI with lognormal theory for multi-beam (8-beam) measurements made on (a) August 4, 2000, and (b) September 13 through 15, 2000.

The quasi-frequency, $\nu 0$, values (see Section II) determined from the temporal power spectral density have been reported for all the scintillation measurements reported in Tables A-1, A-2, and A-3. Figure 13 shows the distribution of quasi-frequencies at TMF and SP, with TMF being lower. The quasi-frequency can be used to determine the mean number of fades per second and the mean fade duration. These were computed, and the distributions are shown in Fig. 14. Consistent with the lower quasi-frequency values, the mean number of fades per second and the average fade duration are lower for the signal received at TMF. Physically, the quasi-frequency is the inverse of the time that it takes an atmospheric turbulence cell to traverse the receiving aperture and, since this is larger at TMF, the frequency is expected to be lower.

The results presented in this section address observed scintillation measurements made on the beacon propagating from TMF to SP and the counter-propagating OCD communications laser beam. For the beacon, 8 beams were used. The SIs of the individual beams were found to agree with a heuristic spherical-wave model, with the unconfirmed assertion that a range of C_n^2 values was encountered during our measurements. An increasing number of co-propagating beams showed a reduction in SI. The exact mechanism responsible for the reduction requires further analysis. The counter-propagating communications laser beam displayed SI values consistent with aperture averaging. Thus, the strategy for mitigating

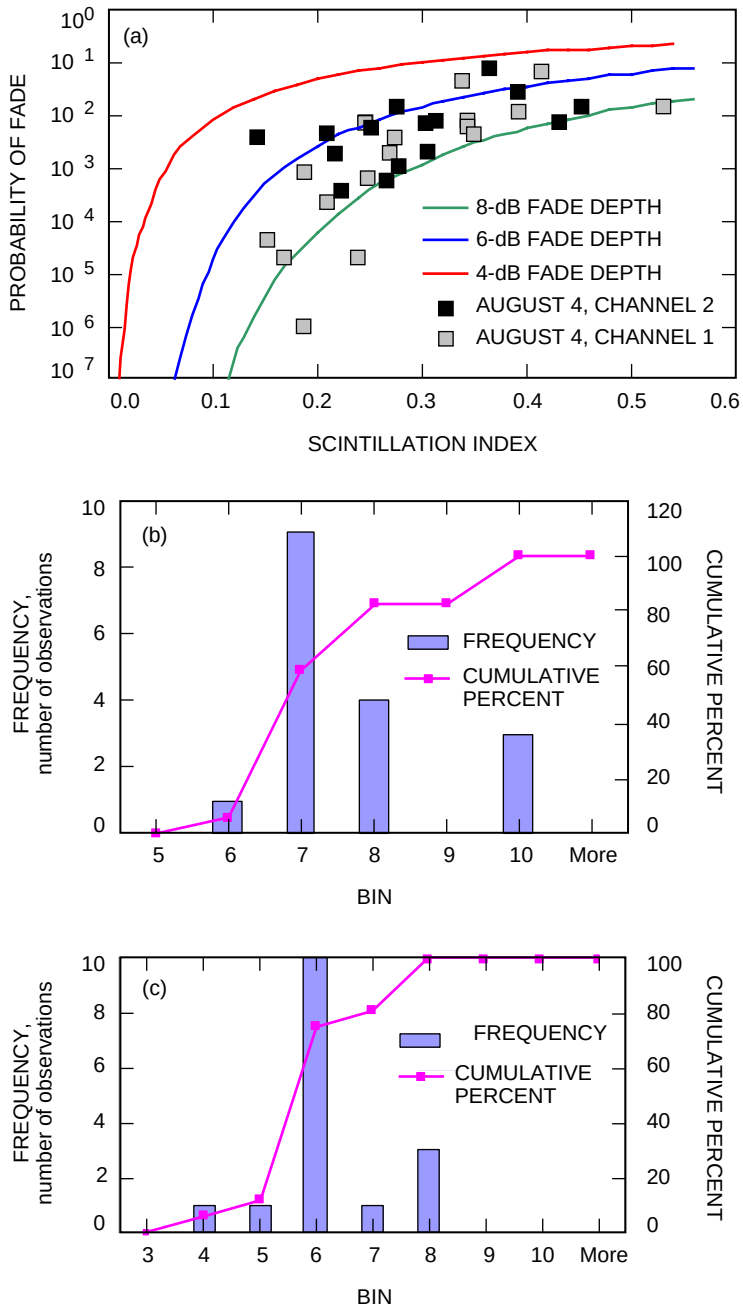

Fig. 12. Data obtained on August 4: (a) a comparison of the theoretical lognormal fade characteristics along with data, and histograms of the measured fade depths for (b) channel 2 and (c) channel 1. The histograms corroborate the comparisons apparent in (a).

scintillation effects by multi-beam averaging on the uplink and aperture averaging on the downlink was validated. Furthermore, the multi-beam and aperture-averaged signals recorded at either end of the link conform well to lognormal statistics. A comparison between the measured and theoretically predicted lognormal fade statistics showed good agreement, with allowance for artifacts introduced by the measurement technique used. Finally, aperture averaging provides for lower mean fade durations and a lower number of fades per second than does multi-beam averaging.

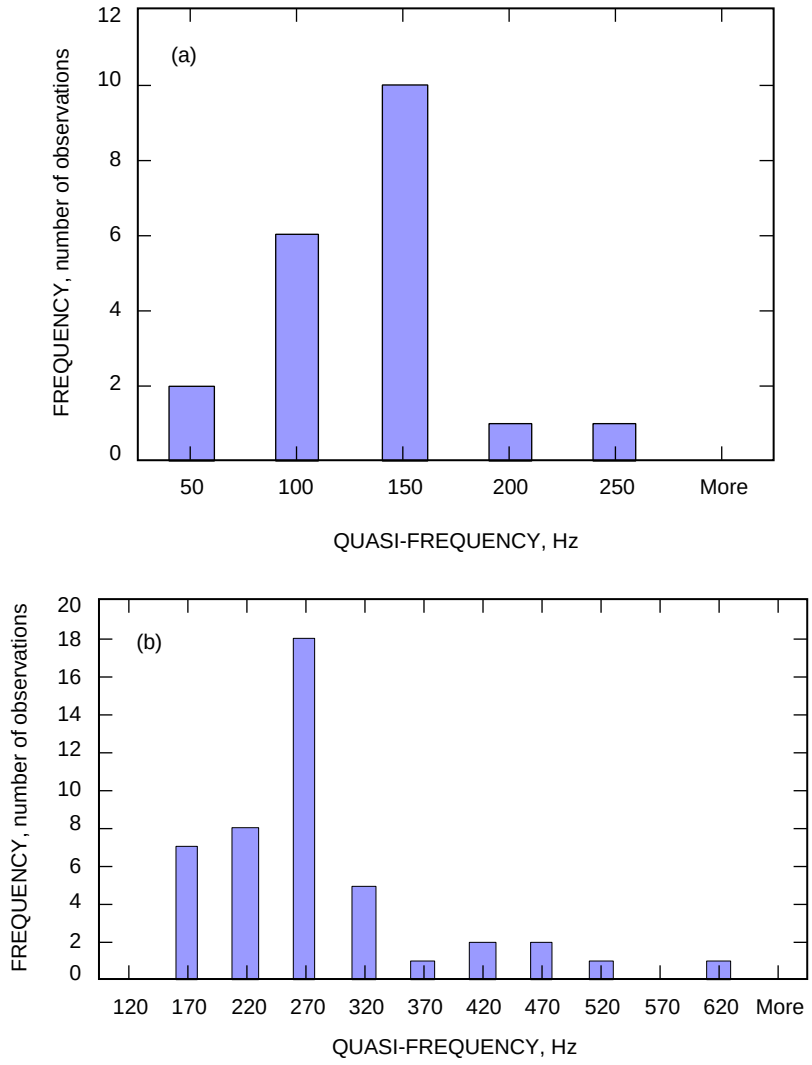

Fig. 13. Distribution of quasi-frequencies determined from the temporal power spectral density of the irradiance fluctuations at (a) TMF and (b) SP.

V. Conclusions

The results of a 46.8-km mountain-top-to-mountain-top optical communications link demonstration, completed in the summer of 2000, have been reported. The optical link was configured to transmit a 780-nm continuous-wave beacon comprised of 8 mutually incoherent co-propagating multi-mode diode laser beams from TMF to SP while transmitting back an 852-nm laser emitted by the OCD. At SP, a pair of 8.5-cm-aperture-diameter spotting telescopes equipped with APDs were used to receive and record the beacon signal. At TMF, a 60-cm-aperture telescope was used to collect the 852-nm communications laser signal. The mean received power at either end of the link agreed well with the best- and worst-case bounds predicted by link analysis. A noteworthy observation of the signal received at TMF was the nearly 28-dB variation that could be sensed between the beam arriving on-axis versus being pointed significantly off-axis so that the second Airy ring could be sensed. The intensity profile of the individual beacon multi-mode beacon beams measured at SP provides strong evidence that the beam-intensity profile launched into the atmosphere is preserved across the atmospheric path. The beacon beam divergences measured on 3 of the 8 beams indicated divergences of 160 to 340 μrad as compared to a design goal of 120 μrad.

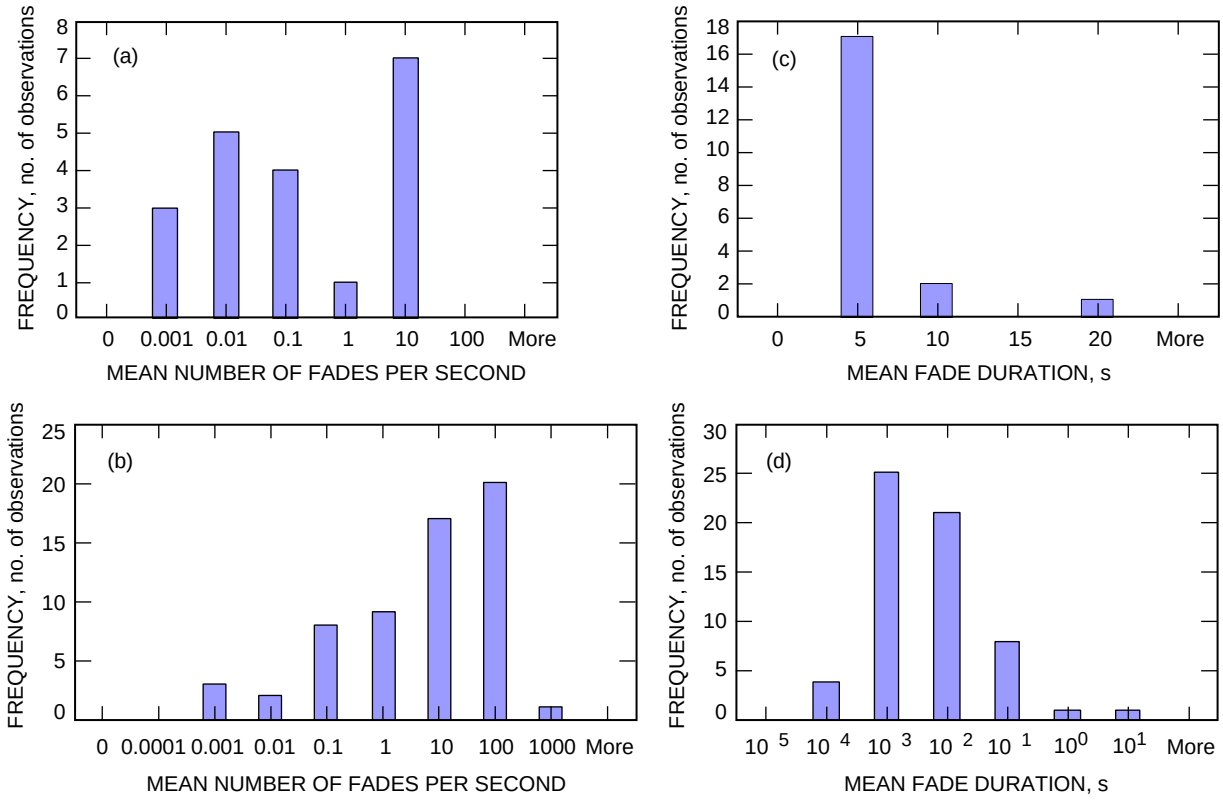

Fig.14. Distribution of the mean number of fades per second at (a) TMF and (b) SP, and of the mean fade duration determined from scintillation data gathered at (c) TMF and (d) SP.

The source of the apparent discrepancy arises from the fact that the optical design approximates the laser energy exiting the fiber core as being uniformly distributed, whereas in reality the beam energy displays numerous "hot-spots" that are smaller in diameter than the fiber-core diameter and that dominate the actual beam divergence. Irradiance fluctuations were recorded for $N = 1, 2, 4, 6$, and 8 beams at SP. The SI measurements on individual beams are consistent with a heuristic theoretical model. A decrease in the SI was observed, and the decrease appeared to scale as $\sqrt{N}$. A numerical convolution of the individual beam lognormal PDFs did not compare favorably with the measured multi-beam PDF. At this time, a sound theoretical explanation of the multi-beam scintillation index reduction is pending. The aperture-averaged SI measured for the 852-nm beam received at TMF compared well with the predicted bounds of 0.18 to 0.3. Based upon the SI values, the fade statistics observed in the recorded data were found to agree well with a theoretical prediction based upon lognormal intensity distribution. The same was found to be true for the multi-beam beacon intensity and fade statistics.

References

[1] A. Biswas, J. Ceniceros, M. Novak, M. Jeganathan, A. Portillo, D. Erickson, J. Depew, B. Sanii, and J. Lesh, "45 km Horizontal Path Optical Link Experiment," *Free-Space Laser Communications Technologies XI, Proceedings of SPIE*, G. S. Mecherle, ed., vol. 3615, pp. 43–53, 1999.

[2] A. Biswas and S. Lee, "Ground-to-Ground Optical Communications Demonstration," *The Telecommunications and Mission Operations Progress Report 42-141, January–March 2000*, Jet Propulsion Laboratory, Pasadena, California, pp. 1–31, May 15, 2000.
http://tmo.jpl.nasa.gov/tmo/progress_report/42-141/141G.pdf

[3] A. Biswas, M. W. Wright, B. Sanii, and N. A. Page, "45 km Horizontal Path Optical Link Demonstrations," *Free-Space Laser Communications Technologies X, Proceedings of SPIE*, G. S. Mecherle, ed., vol. 4272, pp. 60–71, 2001. Provisional Patent CIT File No. 3333-P filed on November 21, 2000 for NPO-21119.

[4] L. C. Andrews and R. L. Phillips, *Laser Beam Propagation through Random Media*, Bellingham, Washington: SPIE Optical Engineering Press, chapters 6 and 7, 1998.

[5] R. R. Beland, "Propagation through Atmospheric Optical Turbulence," *The Infrared and Electro-Optical Systems Handbook*, vol. 2, *Atmospheric Propagation of Radiation*, F. G. Smith, ed., pp. 157–229, 1993.

[6] R. E. Hufnagel, "Propagation through Atmospheric Turbulence," *The Infrared Handbook*, W. L. Wolfe and G. J. Zissis, eds., Office of Naval Research, Department of Navy, Environmental Research Institute of Michigan, pp. 6-1–6-56, 1985.

[7] V. Chan and S. Bloom, "Results of 150 km, 1 Gbps Lasercom Validation Experiment Using Aircraft Motion Simulator," *Free-Space Laser Communications Technologies X, Proceedings of SPIE*, G. S. Mecherle, ed., vol. 2699, pp. 60–70, 1998.

[8] P. A. Lightsey, "Scintillation in Ground-to-Space and Retroreflected Laser Beams," *Opt. Eng.*, vol. 33, pp. 2535–2543, 1994.

[9] J. D. Shelton, "Turbulence-Induced Scintillation on Gaussian-Beam Waves: Theoretical and Observations from a Laser Illuminated Satellite," *J. Opt. Soc. Am. A*, vol. 12, pp. 2172–2181, 1995.

[10] M. Jeganathan, M. Toyoshima, K. Wilson, J. James, G. Xu, and J. Lesh, "Data Analysis Results form the GOLD Experiments," *Free-Space Laser Communications Technologies IX, Proceedings of SPIE*, G. S. Mecherle, ed., vol. 2990, pp. 70–81, 1997.

[11] M. Jeganathan, K. E. Wilson, and J. R. Lesh, "Preliminary Analysis of Fluctuations in the Received Uplink-Beacon-Power Data Obtained from the GOLD Experiments," *The Telecommunications and Data Acquisition Progress Report 42-124, October–December 1995*, Jet Propulsion Laboratory, Pasadena, California, pp. 20–32, February 15, 1996.
http://tmo.jpl.nasa.gov/tmo/progress_report/42-124/124J.pdf

[12] J. L. Bufton, R. S. Iyer, and L. S. Taylor, "Scintillation Statistics Caused by Atmospheric Turbulence and Speckle in Satellite Laser Ranging," *Applied Optics*, vol. 16, pp. 2408–2413, 1977.

[13] L. C. Andrew, R. L. Phillips, C. Y. Hopen, and M. A. Al-Habash, "Theory of Optical Scintillation," *J. Opt. Soc. Am. A*, vol. 16, pp. 1417–1429, 1999.

[14] K. E. Wilson, A. Biswas, S. Bloom, and V. Chan, "Effect of Aperture Averaging on a 570 Mbps 42 km Horizontal Path Optical Link," *Atmospheric Propagation and Remote Sensing IV, Proceedings SPIE*, J. C. Dainty, ed., vol. 2471, p. 244–253, April 1995.

[15] C. Higgs, H. Barclay, D. Murphy, and C. A. Primmerman, "Multibeam Illumination," *Lincoln Laboratory Journal*, vol. 11, pp. 8–22, 1998.

[16] I. I. Kim, H. Hakakha, P. Adhikari, E. Korevaar, and A. K. Mazumdar, "Scintillation Reduction Using Multiple Transmitters," *Free-Space Laser Communications Technologies X, Proceedings of SPIE*, G. S. Mecherle, ed., vol. 2990, pp. 102–113, 1997.

[17] R. L. Phillips and L. C. Andrews, "Measured Statistics of Laser-Light Scattering in Atmospheric Turbulence," *J. Opt. Soc. Am.*, vol. 17, pp. 1440–1445, 1981.

[18] K. Kiasaleh, "On the Probability Density Function of Signal Intensity in Free-Space Optical Communications Systems Impaired by Pointing Jitter and Turbulence," *Optical Engineering*, vol. 33, pp. 3748–3757, 1994.

[19] H. Weichl, *Laser Beam Propagation in the Atmosphere*, R. F. Potter, ed., Bellingham, Washington: SPIE Optical Engineering Press, vol. TT-3, pp. 60–63, 1989.

[20] P. Duffett-Smith, *Practical Astronomy with Your Calculator*, Cambridge, United Kingdom: Cambridge University Press, pp. 36–65, 1981.

[21] M. Jeganathan and S. Monacos, "Performance Analysis and Electronics Packaging of the Optical Communications Demonstrator," *Free-Space Laser Communications Technologies XI, Proceedings of SPIE*, G. S. Mecherle, ed., vol. 3266, pp. 33–41, 1998.

[22] A. Berk, L. S. Bernstein, G. P. Anderson, P. K. Acharya, D. C. Roberson, H. H. Adler, and S. M. Golden, "MODTRAN Cloud and Multiple Scattering Upgrades with Applications to AVIRIS," *Remote Sensing of Environment*, vol. 65, pp. 367–375, 1998.

[23] M. Born and E. Wolf, *Principles of Optics*, 7th edition, Cambridge, United Kingdom:: Cambridge University Press, pp. 439–443, 1993.

[24] R. J. Hill and G. R. Ochs, "Inner-Scale Dependence of Scintillation Variances Measured in Weak Scintillation," *J. Opt. Soc. Am.*, vol. A9, pp. 1406–1411, 1992.

[25] E. A. Murphy, R. R. Beland, J. H. Brown, and P. J. Thomas, "Scintillation and Turbulence Measurements: Comparisons over a Horizontal Path," *Optical, Infrared, and Millimeter Wave Propagation Engineering*, SPIE, vol. 926, pp. 352–359, 1988.

Appendix

Scintillation Characteristics for 780-nm and 852-nm Laser Beams Traversing a 46-km Horizontal Atmospheric Path

Tables A-1 through A-3 present a tabulation of scintillation characteristics for 780-nm and 852-nm laser beams traversing a 46-km horizontal atmospheric path.

Table A-1. Summary of 780-nm beacon-characterization results (June 28 through 30, 2000) using the spotting telescopes equipped with APDs to receive the signal after the laser beam has propagated 46.8 km from TMF to SP.

Beam/ channel	Mean signal, V	Standard deviation, V	SI	Fade, percent	Full dynamic range, dB	Half dynamic range, dB	Quasi-frequency ν_0
June 28, 2000, 03:21 to 04:34 a.m.							
1	1.834	1.90	1.08	1.6500	18.2	13.6	42
2	0.113	0.12	1.07	1.9000	22.4	11.5	192
3	0.061	0.06	0.88	3.9000	21.7	11.9	386
4	0.018	0.014	0.62	24.0000	23	13.6	1294
5	0.092	0.09	0.91	3.3000	19.6	10.7	284
6	0.126	0.12	0.87	2.4000	17.6	8.0	240
7	0.799	0.94	1.40	0.3000	22.7	13.0	46
8	2.138	2.32	1.18	0.5400	18.3	14.3	35
23	0.183	0.179	0.95	0.6880	19.5	9.7	126
45	0.896	0.909	1.03	0.1900	23.1	13.5	46
4523	0.206	0.136	0.43	0.0400	18.8	12.4	178
4523	0.379	0.199	0.28	0.0000	16.5	10.0	129
123678	0.554	0.330	0.36	0.0000	15.9	9.0	90
12345678	0.700	0.344	0.24	0.0000	12	6.7	82
12345678	0.637	0.315	0.25	0.0000	13.99	7.6	91
June 29, 2000, 0:00 to 2:42 a.m.							
1	0.753	1.062	1.99	16.0000	21.1	9.7	91
2	0.978	1.363	1.94	6.3000	21.1	10.9	89
3	0.590	0.777	1.73	18.2000	21.8	8.7	99
4	0.990	1.272	1.65	6.3000	21.1	10.9	80
5	0.863	1.159	1.81	8.1000	21.2	10.3	89
6	0.343	0.416	1.47	0.8000	21.4	9.3	91
7	0.415	0.567	1.87	28.7000	20.6	7.2	150
8	0.183	0.232	1.61	3.4000	20.7	6.6	158
5678	0.900	0.832	0.85	0.6000	21.2	10.5	93
1234	1.785	1.549	0.75	0.0300	21.2	13.5	64
1234	0.894	0.788	0.78	0.7900	20.7	10.5	92
123456	0.995	0.871	0.77	0.4340	20.9	10.9	84
123456	1.454	1.098	0.57	0.1720	20.7	12.6	70
12345678	2.125	1.611	0.58	0.0160	21.1	14.2	54
12345678	1.372	1.085	0.63	0.0060	21.3	12.3	66

Table A-1 (contd).

Beam/ channel	Mean signal, V	Standard deviation, V	SI	Fade, percent	Full dynamic range, dB	Half dynamic range, dB	Quasi-frequency ν_0
June 29, 2000, 22:15 p.m., to June 30, 2000, 02:30 a.m.							
5/B	0.677	0.788	1.36	14.5000	19.3	9.3	87
5/A	0.548	0.486	0.79	7.4200	15.9	6.6	140
6/B	1.168	1.273	1.19	2.0000	21.1	11.7	60
6/A	0.662	0.726	1.20	3.8000	19	7.4	97
7/B	1.417	1.27	0.80	0.7000	21.1	12.5	57
7/A	0.81	0.717	0.78	0.7500	18.3	8.3	96
8/B	1.128	1.031	0.84	0.8900	21.1	11.5	66
8/A	0.708	0.632	0.80	0.7000	16.7	7.7	106
23/B	1.132	1.155	1.04	1.4500	21.8	11.5	63
23/A	0.602	0.476	0.63	1.1000	15.1	7.0	141
23/B	0.798	0.784	0.97	2.3000	19.6	10.0	87
23/A	0.753	0.665	0.78	0.4100	17.4	7.9	104
34/B	1.132	1.01	0.80	0.9900	20.5	11.5	65
34/A	0.897	0.697	0.60	0.1000	17.7	8.7	96
2345/B	1.354	0.951	0.49	0.1100	21.1	12.3	79
2345/A	0.931	0.621	0.45	0.0080	16.9	8.9	111
2345/B	1.335	1.047	0.62	0.0820	21.1	12.3	73
2345/A	0.993	0.79	0.63	0.0780	18.8	9.1	87
234567/B	2.577	1.761	0.47	0.0000	18.2	12.1	49
234567/A	1.611	1.068	0.44	0.0000	17.2	9.0	69
234567 /B	2.663	1.667	0.39	0.0000	21.2	15.3	51
234567/A	1.64	1.066	0.42	0.0000	19.4	11.3	69
12345678/B	2.148	1.411	0.43	0.0020	21.1	14.3	54
12345678/A	1.311	0.781	0.36	0.0000	17.4	10.3	89
12345678/B	2.056	1.337	0.42	0.0000	21.4	14.1	58
12345678/A	1.279	0.729	0.33	0.0000	18.6	10.2	97
12345678/B	2.149	1.449	0.45	0.0000	21.2	14.3	55
12345678/A	1.336	0.861	0.42	0.0000	17	8.2	82
12345678/B	0.754	0.499	0.44	0.3640	17.9	9.8	126
12345678/A	0.597	0.325	0.30	0.1660	14.5	6.9	202
12345678/B	0.733	0.466	0.41	0.3000	16.5	9.7	135
12345678/A	0.539	0.314	0.34	0.0000	18.8	6.5	209
12345678/B	0.678	0.489	0.52	1.1800	17.4	9.3	128
12345678/A	0.54	0.298	0.30	0.0740	14.5	6.5	219

Table A-2. Summary of 852-nm OCD beam-characterization results (August 4 and September 14 and 15, 2000) using a 0.6-m telescope at TMF to receive the signal that was measured using a p-i-n photodiode at the Coudé focus.

Date	Mean signal, V	Standard deviation, V	SI	Fade, percent	Full dynamic range, dB	Half dynamic range, dB	Quasi-frequency λ_0
9-15-00	3.14	1.88	0.36	0.0300	17.99	12.03	137.81
9-15-00	1.14	0.83	0.53	0.4900	19.02	9.8	142.98
9-15-00	1.09	0.82	0.57	1.1200	19.1	9.6	139.14
9-15-00	1.11	0.84	0.58	4.8000	18.3	9.6	140.12
9-15-00	1.06	0.823	0.6	10.5000	18.6	9.4	144.27
9-15-00	1.07	0.75	0.49	2.7600	17.83	9.6	142.03
9-15-00	1.39	0.66	0.22	0.0002	18.7	10.6	141.55
9-15-00	0.94	0.68	0.53	3.0500	17.95	9.03	141.97
9-14-00	2.55	1.45	0.33	0.0002	17.9	11.1	111.66
9-14-00	2.7	1.51	0.31	0.0002	17.9	11.3	114.61
8-04-00	2.69	1.45	0.29	0.1000	14.87	8.25	81.59
8-04-00	2.29	1.22	0.29	0.2900	14.87	7.56	88.35
8-04-00	3.58	1.86	0.27	0.1000	14.9	9.5	49.48
8-04-00	3.59	1.87	0.27	0.1200	14.93	9.52	47.12
8-04-00	0.75	0.35	0.21	0.0800	15.95	9.7	202.24
8-04-00	0.77	0.37	0.23	0.0500	15.38	9.8	190.31
8-04-00	0.85	0.37	0.19	0.0002	14.79	9.27	94.98
8-04-00	0.79	0.38	0.23	0.0002	17.56	11.2	86.91
8-04-00	0.86	0.36	0.17	0.0002	13.48	8.52	70.61
8-04-00	0.8	0.33	0.18	0.0002	15.46	9.97	58.69

Table A-3. Summary of 780-nm beacon-characterization results (August 3 and 4, 2000) using the spotting telescopes equipped with APDs to receive the 8-beam beacon that propagated 46.8 km from TMF to SP.

Number of beams (channel)	Mean signal, V	Standard deviation, V	SI	Fade, percent	Full dynamic range, dB	Half dynamic range, dB	Quasi-frequency ν_0
August 3 and 4, 2000							
8 (1)	0.040	0.026	0.41	6.258	15.3	5.2	314
8 (2)	0.034	0.021	0.40	2.400	15.2	5.3	346
8 (1)	0.060	0.037	0.39	1.146	15.6	6.9	181
8 (2)	0.055	0.038	0.46	0.378	18.4	7.4	227
8 (1)	0.058	0.034	0.34	4.222	16.3	6.8	209
8 (2)	0.055	0.034	0.42	2.072	16.4	7.3	251
8 (1)	0.057	0.034	0.35	0.422	17.4	6.8	221
8 (2)	0.048	0.027	0.31	0.138	15.5	6.8	284
8 (1)	0.054	0.032	0.35	0.750	15.3	6.6	207
8 (2)	0.053	0.035	0.44	0.148	18.5	7.2	231
8 (1)	0.058	0.034	0.34	0.564	15.2	6.8	224
8 (1)	0.049	0.028	0.32	0.158	15.9	6.9	266
8 (2)	0.061	0.032	0.27	0.360	16.9	7.0	251
8 (1)	0.061	0.034	0.31	0.058	17.8	7.8	276
8 (2)	0.059	0.030	0.25	0.226	16.4	6.9	243
8 (1)	0.067	0.035	0.27	0.184	14.2	6.8	270
8 (2)	0.064	0.034	0.27	0.066	15.9	6.6	270
8 (1)	0.071	0.036	0.25	0.058	14.6	7.1	209
8 (2)	0.075	0.038	0.26	0.036	15.7	7.3	291
8 (1)	0.075	0.029	0.15	0.004	13.1	7.3	191
8 (2)	0.064	0.024	0.14	0.020	12.9	6.6	347
8 (1)	0.077	0.031	0.17	0.002	12.8	7.4	185
8 (2)	0.077	0.036	0.22	0.006	15.9	7.4	229
8 (1)	0.062	0.027	0.19	0.078	13.1	6.5	201
8 (2)	0.062	0.028	0.21	0.004	13.4	6.5	267
8 (1)	0.123	0.056	0.21	0.002	15.8	9.5	122
8 (2)	0.107	0.055	0.27	0.002	16.1	8.9	155
8 (1)	0.124	0.053	0.19	0.000	13.5	6.8	165
8 (1)	0.101	0.048	0.22	0.0000	16.5	9.2	166
8 (2)	0.133	0.065	0.24	0.002	17.7	9.8	192
8 (1)	0.103	0.054	0.27	0.000	17.2	9.3	180
8 (2)	0.059	0.043	0.53	1.418	16.6	6.2	163

Table A-3 (contd).

Number of beams ([define])	Mean signal, V	Standard deviation, V	SI	Fade, percent	Full dynamic range, dB	Half dynamic range, dB	Quasi-frequency ν_0
			September 13, 2000				
8 (1)	0.069	0.030	0.18	0.450	9.8	3.6	437
8 (2)	0.098	0.049	0.25	0.090	11.9	5.1	301
8 (1)	0.066	0.024	0.13	0.310	7.5	3.4	540
8 (2)	0.105	0.046	0.19	0.080	10.1	5.5	321
8 (1)	0.055	0.020	0.13	0.000	13.5	8.4	229
8 (2)	0.091	0.044	0.23	5.600	10.0	3.5	155
8 (1)	0.044	0.019	0.18	5.1000	7.9	3.6	238
8 (2)	0.090	0.046	0.26	0.0100	18.2	11.7	163
8 (1)	0.044	0.019	0.20	0.0020	18.9	13.4	261
8 (2)	0.059	0.025	0.17	0.0040	13.4	9.3	301
			September 14, 2000				
8 (1)	0.184	0.100	0.30	1.7000	20.6	11.9	517
8 (2)	0.188	0.098	0.27	1.9000	18.0	11.0	593
8 (1)	0.182	0.088	0.23	0.2500	20.3	11.8	413
8 (2)	0.174	0.093	0.28	4.9000	14.5	7.7	643
8 (1)	0.200	0.085	0.18	0.0020	16.7	8.2	266
8 (2)	0.183	0.099	0.29	4.4000	14.2	7.9	602
8 (1)	0.207	0.088	0.18	0.0060	14.9	8.4	260
8 (2)	0.170	0.083	0.24	1.2000	13.3	7.5	443
8 (1)	0.189	0.081	0.18	0.0000	14.5	8.0	234
8 (2)	0.167	0.085	0.26	1.2000	14.9	7.4	413
8 (1)	0.184	0.084	0.21	0.0060	14.4	7.9	225
8 (2)	0.170	0.097	0.33	3.6000	15.6	7.6	552
8 (1)	0.161	0.077	0.23	0.0300	15.3	7.3	265
8 (2)	0.172	0.096	0.31	3.3000	16.0	7.6	537
			September 15, 2000				
8 (1)	0.0910	0.0586	0.41	19.70	19.7	19.5	1255
8 (1)	0.0839	0.0540	0.41	23.80	23.8	19.2	1295
8 (1)	0.0724	0.0460	0.40	32.00	32.0	19.5	1392
8 (1)	0.0922	0.0582	0.40	28.60	28.6	18.9	1415
8 (1)	0.0896	0.0561	0.39	31.55	31.6	18.5	1427
8 (1)	0.2517	0.1790	0.51	4.35	4.4	21.0	627
8 (1)	0.2497	0.1750	0.49	4.03	4.0	20.8	643
8 (1)	0.3082	0.1924	0.39	2.03	2.0	17.3	608
8 (1)	0.3685	0.2370	0.41	1.47	1.5	18.6	502